

Electron-impact study of PO₂ using the *R*-matrix method

Anand Bharadvaja,^{*} Savinder Kaur,[†] and K. L. Baluja[‡]

Department of Physics and Astrophysics, University of Delhi, Delhi 110007, India

(Received 31 March 2013; published 6 June 2013)

The *R*-matrix approach is used to study the electron scattering from PO₂ radical at low electron impact energies. The elastic scattering phenomenon is studied in static-exchange, one-state and many-states close-coupling approximation. The elastic differential cross sections, corresponding momentum-transfer cross sections, and collision frequency are calculated in the one-state configuration interaction approximation only. Calculations reveal a stable bound state of PO₂⁻ having symmetry ¹A₁, a configuration of ...8a₁², ...2b₁², ...5b₂², ...1a₂², and vertical electron affinity of 2.94 eV. The excited state of anion PO₂⁻ having symmetry ³B₁ is also just bound relative to the ground state of PO₂ at its equilibrium geometry. The shape, core-excited, and Feshbach resonances are analyzed in different symmetries up to 7 eV. The partial waves up to $l = 4$ are used to represent continuum electron. The converged cross sections are obtained for the partial waves having l greater than 4 by applying Born correction. Certain interesting spectroscopic properties of radical are also reported.

DOI: 10.1103/PhysRevA.87.062703

PACS number(s): 34.80.Bm, 34.80.Gs, 34.80.Ht

I. INTRODUCTION

Electron-molecule collisions play a central role in a variety of naturally occurring and laboratory-produced phenomena. The phenomenon is of fundamental importance in atmospheric physics, plasma physics, laser physics, modeling of stellar atmosphere, plasma, radiation physics, and chemistry. The electron-molecule collisions at low energies are a major cause of radiation damage in biological systems [1]. Processes such as plasma etching, plasma modeling, plasma reactors, etc. require accurate and reliable values of cross sections. The accurate simulation of electron-molecule scattering at low scattering energies and also its analysis for polyatomic molecules is a formidable challenge. This is due to several reasons, such as loss of spherical symmetry in molecular systems and difficulty in accurate representation of the target wave function. Electron-molecule scattering is also characterized by rotational, vibrational, excitation, dissociation, and dissociative attachment or recombination processes in addition to electronic excitation and ionization processes. The success in the study of the scattering process is attributed to advancements made in experimental and computational methods [2,3]. The study of resonances arising in collision phenomena provide vital information on dissociative attachment.

The study of the PO₂ radical is important to understand the combustion chemistry of organophosphorus agents [4–7], fire retardants [8,9], chemiluminescence phenomena [10–13], as well as DNA modeling [14]. The spectroscopic study of ground and some excited states of PO₂ [15–23] have been studied by a variety of methods [24–34]. Here, we study the electron-PO₂ collision process.

This work reports the different cross sections at energies up to 10 eV using the UK molecular *R*-matrix code [35,36]. The electron scattering calculations from PO₂ are performed using static-exchange (SE) and close-coupling approximations (one-state and many-states). The resonance phenomenon arising due to the occupation of unoccupied orbitals by the incoming electron is also analyzed in great detail.

II. METHOD

A. Theory

The *R*-matrix theory has been discussed earlier [37]. The main idea of the *R*-matrix approach is to divide the configuration space into inner and outer regions. The target states include correlations and are represented by configuration interaction (CI) effects. The target and continuum orbitals are represented by a set of Gaussian orbitals and are orthogonalized using Schmidt orthogonalization. The continuum molecular orbitals are then orthogonalized among themselves using symmetric or Löwdin orthogonalization. This removes the linearly dependent functions [35,38].

In the inner region, the $N + 1$ scattering system is represented by a CI-type basis expansion [39]

$$\begin{aligned} \Psi_k^{N+1} = & A \sum_i \phi_i^N(x_1, \dots, x_N) \sum_j \xi_j(x_{N+1}) a_{ijk} \\ & + \sum_m \chi_m(x_1, \dots, x_N, x_{N+1}) b_{mk} \end{aligned} \quad (1)$$

where, A is an antisymmetrization operator, x_N is the coordinate of the N th electron, ϕ_i^N is the i th target state, ξ_j are the continuum orbitals basis of the scattering electron, k represents a particular *R*-matrix basis function. The coefficients a_{ijk} and b_{mk} are determined by matrix diagonalization. The continuum orbitals basis do not vanish on the boundary unlike the bound orbital basis function. The χ_m are $(N + 1)$ electron correlation functions constructed from the bound orbitals; and ensure the completeness of the basis function when the continuum orbital basis is orthogonalized to the bound electron basis. It further allows us to include correlation effects beyond those

*Also at: Bhaskaracharya College of Applied Sciences, University of Delhi, New Delhi 110075; anand_bharadvaja@yahoo.com

†Also at: Department of Physics, SGTB Khalsa College, University of Delhi, Delhi 110007; sk_savinder2005@yahoo.co.in

‡kl_baluja@yahoo.com

TABLE I. Comparison of ionization potential of PO_2 (in eV) with other works.

Ionization potential	Reference
10.75 ± 0.01	[15]
12.78	[40]
10.6 ± 0.25	[42]
10.5 ± 0.1	[43]
11.0 ± 0.5	[44]
12.88	Present work

included in the first expansion. These additional correlation effects arise from virtual excitations to higher electronic states. The configuration state functions (CSFs) in the second term of Eq. (11) are constructed by allowing the scattering electron to occupy any of the target occupied or virtual orbitals. This term is also responsible for the polarization effects in the close coupling approximations.

The R -matrix boundary radius is taken as $12a_0$ and is centered at the PO_2 center of mass. This sphere encloses the entire charge cloud of the occupied and virtual molecular

orbitals. At $12a_0$, the amplitudes of the molecular orbitals are less than $10^{-5} a_0^{-3/2}$. All calculations are performed in the fixed-nuclei approximation.

B. PO_2 target model

The PO_2 radical belongs to C_{2v} symmetry having X^2A_1 as the ground state. The radical is a prolate asymmetric top. The HF ground-state configuration of the PO_2 molecule is $\dots 8a_1^1 \dots 2b_1^1 \dots 5b_2^2 \dots 1a_2^2$. The frontier unoccupied orbitals such as $3b_1$, $9a_1$, and $6b_2$ are generated in a self-consistent field (SCF) procedure. The double zeta plus polarization (DZP) Gaussian basis set [39] contracted to (12,8,1)/(9,6,1) for P atom and for O atoms are used. The calculations are performed at experimental value of $R_{\text{PO}} = 1.4665 \text{ \AA}$ and $\angle \text{OPO} = 135.283^\circ$ [25].

The vertical electronic affinity (VEA) is computed using bound state calculations by including the continuum electron basis functions centered at the origin. The VEA of 2.94 eV corresponds to a stable bound state having 1A_1 symmetry, which is close to the experimental value of 3.42 ± 0.01 eV

TABLE II. State, transition moment (au) and T_v (eV) for excited states of PO_2 at experimental geometry [25].

State	Transition	Vertical		Excitation		Energy	
		Present Work	Cai <i>et al.</i> [23]	Lee <i>et al.</i> [46]		MRCI	
				CIS	CASSCF(1)		
X^2A_1	0.734 29 [†]	0.000	0.0	—	—	—	—
1^2B_2	0.1478	3.070	2.59	3.61	2.47	2.47	—
1^2A_2	—	3.116	2.63	3.93	—	—	—
1^2B_1	0.2109	4.247	3.90	4.80	4.13	4.23	—
2^2A_1	0.5159	5.079	4.64	5.70	4.91	4.77	4.47
2^2B_1	0.4871	5.192	4.56	6.02	5.09	4.91	—
1^4B_2	—	5.567	—	—	—	—	—
2^2B_2	0.067 07	5.616	4.0	6.57	5.20	5.10	—
1^4A_2	—	5.672	—	—	—	—	—
2^2A_2	—	6.10	8.57	—	—	—	—
3^2B_2	0.4973	6.922	7.19	—	—	—	—
1^4A_1	—	7.272	—	—	—	—	—
3^4B_1	—	7.518	—	—	—	—	—
3^2A_2	—	7.912	—	—	—	—	—
3^2A_1	0.2773	7.922	5.82	—	—	—	—
4^2A_1	0.3035	7.999	6.12	—	—	—	—
2^4A_2	—	8.204	—	—	—	—	—
4^2B_2	0.3762	8.250	9.73	—	—	—	—
4^2B_1	0.1167	8.674	8.7	—	—	—	—
2^4B_2	—	8.870	—	—	—	—	—
3^4A_2	—	9.079	—	—	—	—	—
4^2A_2	—	9.203	—	—	—	—	—
5^2A_2	—	9.334	—	—	—	—	—
5^2A_1	0.3618	9.344	8.45	—	—	—	—
5^2B_1	0.1388	9.599	8.72	—	—	—	—
4^4A_2	—	9.794	—	—	—	—	—
2^4A_1	—	9.903	—	—	—	—	—
6^2A_1	0.5179	9.936	8.54	—	—	—	—
5^2B_2	0.1355	10.04	—	—	—	—	—

[†]dipole moment.

[21]. The 3B_1 symmetry state of anion PO₂ is also just bound at the equilibrium geometry.

The ground-state value of dipole moment 2.31 D obtained in SCF compares well with the value 2.14 D reported by Lohr *et al.* [17]. The difference in the two is due to different basis sets and geometry employed. The inclusion of correlation effects lowers the value of the dipole moment to 1.867 D in many-states calculations. This value, however, differs significantly from the value 0.202 D reported by Esquivel *et al.* [40] using the CISD model. The components of quadrupole moments Q_{20} and Q_{22} obtained are 2.7330 au and 6.083 43 au, respectively.

The vertical ionization potential is determined from the SCF orbital energies using the restricted Hartree-Fock formalism (ROHF) [41]. Thus, the molecular orbital $8a_1$ yields the first ionization energy of 12.88 eV. This value is compared to other works in literature [15,40,42–44] and is presented in Table I.

The ground-state energy of PO₂ obtained in SCF model is -490.452 5390 au while in the one-state CI model it is -490.523 64 au. It gets slightly reduced in many-states close-coupling approximations. The SCF and one-state CI energy values are close to values reported by others [9,17, 18,20,40,45]. The close-coupling model includes correlation effects and thus results in lower spectroscopic values in the many-states model, hence provides a good representation of the target states better than SCF calculations. In the CI model, 14 frozen electrons get distributed in molecular orbitals $1a_1^2 2a_1^2 \dots 4a_1^2 1b_1^2$, $1b_2^2 2b_2^2$ and the remaining 17 electrons move freely in 12 molecular orbitals $5a_1 \dots 9a_1$, $2b_1, 3b_1$, $3b_2 \dots 6b_2$, $1a_2$.

In Table II, we have shown the transition moments and also compared the vertical excitation energies T_v for various excited states of PO₂ with other works. Our T_v values for the low-lying excited states are better than the configuration interaction singles (CIS) values of Lee *et al.* [46]. They match satisfactorily well with the multireference configuration interaction (MRD-CI) calculations of Cai *et al.* [23], and complete active space self-consistent field theory (CASSCF) and multireference configuration interaction (MRCI) levels of Lee *et al.* [46]. The differences in the values of T_v of the target molecule between this and other work [23,46] arise due to the different basis set, the active space, and the correlation effects used. The large value of the transition moment 0.5159 au for the state 2^2A_1 suggests it to be the strongest transition among the low-lying excited states and is in conformity with the observation reported by Lee *et al.* [46].

C. Scattering model

The trial wave function describing the scattering system (electron plus target) is described by 29 target states. Of these 29 states, there are 20 spin doublet and nine spin quartet states. The 20 spin doublet target states have $6A_1$, $4B_1$, $5B_2$, $5A_2$ symmetries whereas the nine spin quartet target states have $2A_1$, $1B_1$, $2B_2$, $4A_2$ symmetries. The scattering calculations are, therefore, performed for singlet and triplet states having A_1, A_2, B_1 , and B_2 symmetries. Continuum orbitals up to g partial wave ($l = 4$) are represented by Gaussians centered at the molecule center of gravity [47].

The partial waves for $l > 4$ are included using a Born correction via a closure approach [48,49] at all energies. The

Shape Resonance in 3B_1

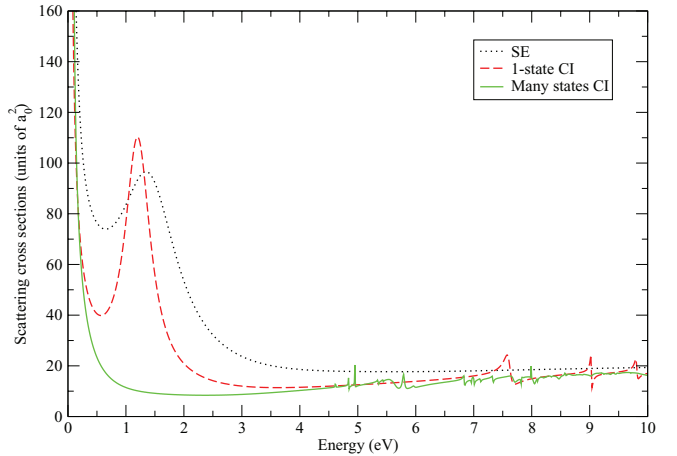


FIG. 1. (Color online) Elastic cross sections of the electron impact on the PO₂ molecule for 3B_1 scattering symmetry state; dotted curve, SE; dashed curve, CI one-state; solid curve, many-states CI.

propagated solutions thus obtained at $50a_0$ are matched with the asymptotic boundary conditions yielding K matrices and hence the integral cross sections.

III. RESULTS

A. Elastic and Inelastic cross sections

Figure 1 shows the elastic cross sections in three different models viz. SE, one-state, and many-states CI model. A sharp resonance is observed in the SE model at 1.35 eV for 3B_1 symmetry of width 0.56 eV. This peak gets lowered to 1.2 eV in the correlated one-state model. In our best model, i.e., the many-states model, the peak vanishes and thus exhibits the bound-state nature of this state. The resonance parameters are further fitted to the cross sections using Breit-Wigner profile.

The total elastic cross sections summed over all symmetries in different models are shown in Fig. 2. The cross sections

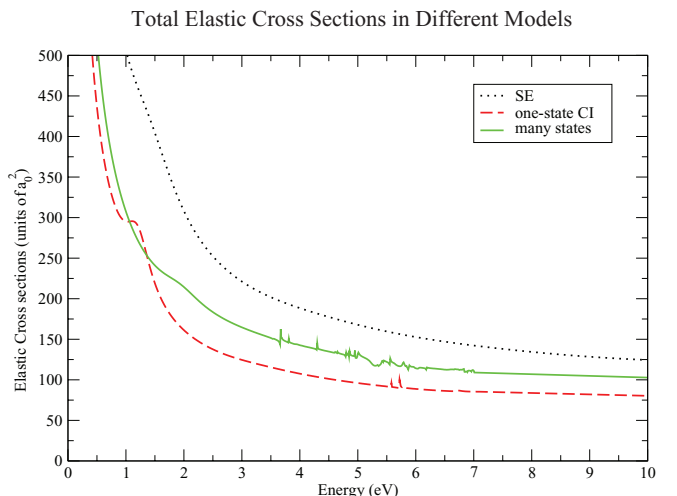


FIG. 2. (Color online) Comparison of total elastic cross sections; dotted curve, SE; dashed curve, one-state CI; solid curve, many-states CI.

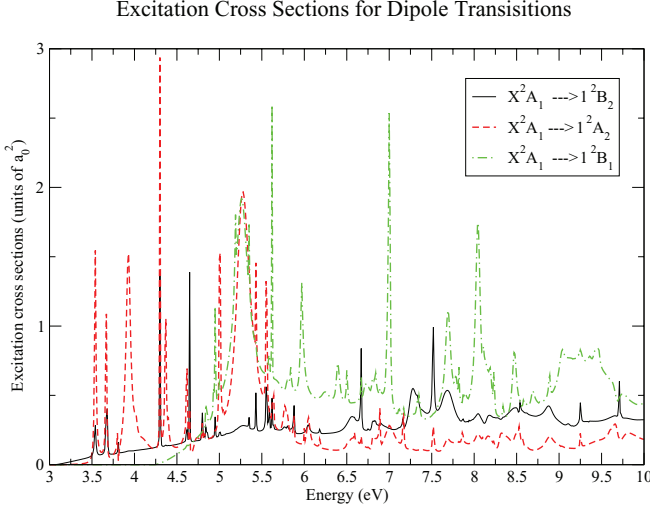


FIG. 3. (Color online) Excitation cross sections from ground state X^2A_1 to (a) 1^2B_2 , solid curve (b) 1^2A_2 , dotted curve, and (c) 1^2B_1 , dashed dotted curve in many-states model.

obtained in SE model are higher than the correlated models represented by the one-state and many-states models.

Figure 3 reports the excitation cross sections for dipole allowed transitions from ground state (X^2A_1) to 1^2B_2 , 1^2A_2 , and 1^2B_1 . A rich structure of resonance is noticed as the atomic constituents of the molecule are all open shell in nature. These resonances are either core excited or Feshbach type.

In Fig. 4, cross sections for dipole allowed transitions from ground state to second excited states having symmetry 2A_1 and 2B_1 are shown. The cross sections from ground state to 2^2B_1 are significantly lower than the ground state to 2^2A_1 transition due to the lower value of its transition moment.

Figure 5 shows cross sections for spin forbidden transitions from $X^2A_1 \rightarrow 1^4A_2$ and $X^2A_1 \rightarrow 1^4B_2$. These cross sections are much smaller than the corresponding dipole allowed transitions. The transition parameter for quartet states is identically zero.

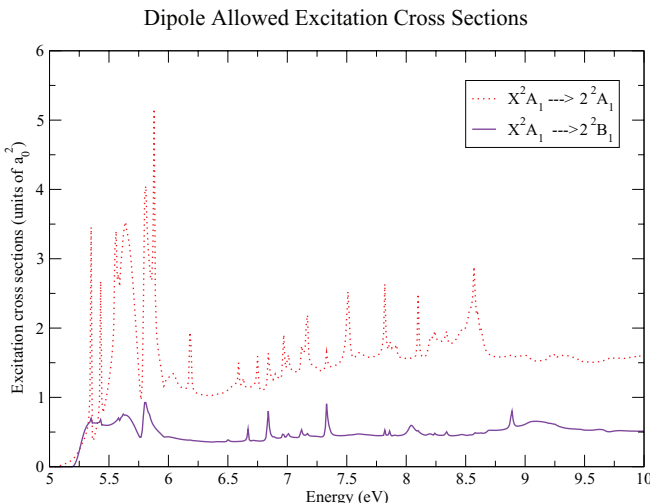


FIG. 4. (Color online) Dipole allowed excitation cross sections from ground X^2A_1 to (a) 2^2A_1 : dashed dotted curve (b) 2^2B_1 : solid curve in many-states model.

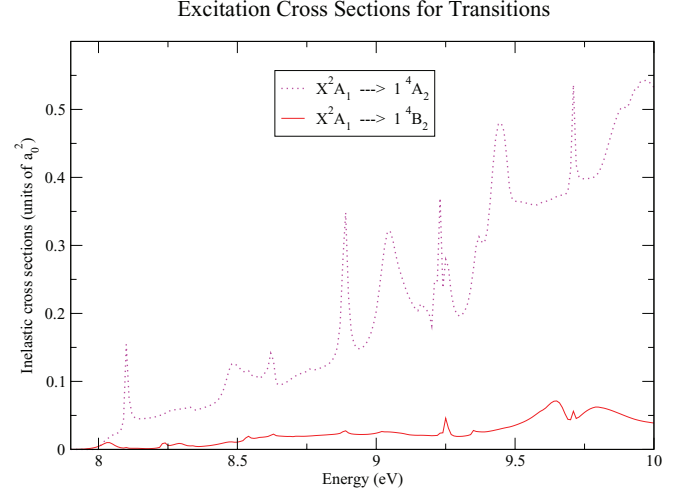


FIG. 5. (Color online) Excitation cross sections from ground X^2A_1 to (a) 1^4A_2 , dashed curve (b) 1^4B_2 , solid curve in many-state model.

1. Shape resonance

It arises when an electron is quasibound to a molecule in its electronic ground state. It decays to the parent state. The resonance is broad in nature. Here, the scattering electron can occupy any of the virtual molecular orbitals such as $3b_1$, $9a_1$, $6b_2$ giving rise to shape resonances in various symmetries. This type of resonance appears only when the electron possesses an angular momentum relative to the target molecule. It is absent in low-energy s -wave scattering ($l = 0$) as the electrons can not be trapped.

2. Core-excited shape resonance (CE)

It is formed when the electron jumps from the inner molecular orbitals to virtual orbitals like $3b_1$, $9a_1$, $6b_2$ and the scattering electron also occupies one of these virtual orbitals. The decay leads to the metastable excited state. The CE are sharper and narrower than shape resonances.

The electron gets promoted from molecular orbitals like $5b_2$, $1a_2$, $4b_2$, and $6a_1$ to generate the excited state electronic configurations. The summary of all resonances including the electronic configuration, resonance energy E_r (eV), and full width half maxima Γ_r (eV) are shown in Tables III–VII.

3. Feshbach resonance (FB)

These are closed channel resonances in which the excited state is energetically not accessible to the electron. The parent state hence lies above the resonance state. The FBs are characterized by narrow peaks.

TABLE III. Shape resonance.

Electronic Configuration of Resonant State	Type	E_r (eV)	Γ_r (eV)
$^3B_1 :: X^2A_1(3b_1)$	SE	1.35	0.56
$^3B_1 :: X^2A_1(3b_1)$	one-state CI	1.2	0.417
$^3B_1 :: X^2A_1(3b_1)$	many-states CI	just bound	—

TABLE IV. Core-excited resonances.

Electronic state configuration	E_r (eV)	Γ_r (eV)	Parent state
$^1B_2 : (X^2A_1)6b_2^1$	3.68	0.011	X^2A_1
$^3B_2 : (X^2A_1)6b_2^1$	3.54	0.025	X^2A_1
$^1B_2 : (\dots)5b_2^18a_1^29a_1^1$	4.11	0.206	$1^2B_2(5b_2 \rightarrow 8a_1)$
$^3B_2 : (\dots)5b_2^18a_1^29a_1^1$	3.67	0.019	$1^2B_2(5b_2 \rightarrow 8a_1)$
$^1B_2 : (\dots)1a_2^18a_1^23b_1^1$	4.31	0.213	$1^2A_2(1a_2 \rightarrow 8a_1)$
$^3B_2 : (\dots)1a_2^18a_1^23b_1^1$	4.30	0.011	$1^2A_2(1a_2 \rightarrow 8a_1)$
$^1B_2 : (\dots)7a_1^18a_1^26b_2^1$	4.64	0.115	$2^2A_1(7a_1 \rightarrow 8a_1)$
$^3B_2 : (\dots)7a_1^18a_1^26b_2^1$	4.63	0.011	$2^2A_1(7a_1 \rightarrow 8a_1)$
$^1B_2 : (\dots)1a_2^18a_1^13b_1^19a_1^1$	4.82	0.022	$2^2B_2(4b_2 \rightarrow 8a_1)$
$^3B_2 : (\dots)1a_2^18a_1^13b_1^19a_1^1$	4.8	0.018	$2^2B_2(4b_2 \rightarrow 8a_1)$
$^1B_2 : (\dots)1a_2^29a_1^16b_2^1$	6.9	0.049	$4^2A_1(6a_1 \rightarrow 8a_1)$
$^3B_2 : (\dots)1a_2^29a_1^16b_2^1$	6.89	0.022	$4^2A_1(6a_1 \rightarrow 8a_1)$
$^1B_1 : (\dots)1a_2^18a_1^26b_2^1$	4.63	0.019	$1^2A_2(1a_2 \rightarrow 8a_1)$
$^3B_1 : (\dots)1a_2^18a_1^26b_2^1$	4.61	0.018	$1^2A_2(1a_2 \rightarrow 8a_1)$
$^1B_1 : (\dots)1a_2^18a_1^26b_2^1$	4.86	0.01	$1^2A_2(1a_2 \rightarrow 8a_1)$
$^3B_1 : (\dots)1a_2^18a_1^26b_2^1$	4.84	0.017	$1^2A_2(1a_2 \rightarrow 8a_1)$
$^1B_1 : (\dots)6a_1^18a_1^23b_1^1$	5.98	0.040	$4^2A_1(6a_1 \rightarrow 8a_1)$
$^3B_1 : (\dots)6a_1^18a_1^23b_1^1$	5.80	0.027	$4^2A_1(6a_1 \rightarrow 8a_1)$
$^1A_2 : (\dots)5b_2^18a_1^23b_1^1$	3.81	0.014	$1^2B_2(5b_2 \rightarrow 8a_1)$
$^3A_2 : (\dots)5b_2^18a_1^23b_1^1$	3.80	0.011	$1^2B_2(5b_2 \rightarrow 8a_1)$
$^1A_2 : (\dots)1a_2^18a_1^29a_1^1$	4.02	0.039	$1^2A_2(1a_2 \rightarrow 8a_1)$
$^3A_2 : (\dots)1a_2^18a_1^29a_1^1$	3.93	0.064	$1^2A_2(1a_2 \rightarrow 8a_1)$
$^1A_2 : (\dots)4b_2^18a_1^2$	4.44	0.017	$2^2B_2(4b_2 \rightarrow 8a_1)$
$^3A_2 : (\dots)4b_2^18a_1^2$	4.36	0.026	$2^2B_2(4b_2 \rightarrow 8a_1)$
$^1A_2 : (\dots)2b_1^18a_1^26b_2^1$	4.95	0.011	$2^2B_1(2b_1 \rightarrow 8a_1)$
$^3A_2 : (\dots)2b_1^18a_1^26b_2^1$	4.93	0.022	$2^2B_1(2b_1 \rightarrow 8a_1)$

B. Ionization cross section

The ionization of a molecule due to electron-impact is fundamental to the study of the electron-molecule collision process modeling of discharge plasma, plasma processing of materials, fusion plasma modeling, designing of mercury-free fluorescent lamps and accelerators, and assessing the efficiency

TABLE VI. Feshbach resonances in resonating states 1B_2 and 3B_2

Resonating state configuration	E_r (eV)	Γ_r (eV)	Parent state
$^1B_2 : (\dots)1a_2^18a_1^19a_1^13b_1^1$	5.77	0.067	$2^2A_2(1a_2 \rightarrow 9a_1)$
$^3B_2 : (\dots)1a_2^18a_1^19a_1^13b_1^1$	5.55	0.022	$2^2A_2(1a_2 \rightarrow 9a_1)$
$^1B_2 : (\dots)6b_2^19a_1^1$	6.05	0.044	$3^2B_2(8a_1 \rightarrow 6b_2)$
$^3B_2 : (\dots)6b_2^19a_1^1$	5.88	0.013	$3^2B_2(8a_1 \rightarrow 6b_2)$
$^1B_2 : (\dots)5b_2^18a_1^13b_1^2$	6.56	0.141	$3^2A_2(5b_2 \rightarrow 3b_1)$
$^3B_2 : (\dots)5b_2^18a_1^13b_1^2$	6.18	0.022	$3^2A_2(5b_2 \rightarrow 3b_1)$
$^1B_2 : (\dots)1a_2^29a_1^16b_2^1$	6.81	0.062	$3^2A_1(8a_1 \rightarrow 9a_1)$
$^3B_2 : (\dots)1a_2^29a_1^16b_2^1$	6.75	0.011	$3^2A_1(8a_1 \rightarrow 9a_1)$

of ion gauges [50–52]. The binary-encounter-Bethe (BEB) model [53,54] combines Mott cross sections with the high- T (kinetic energy of the electron) behavior of the Bethe cross sections. This model requires only the binding and orbital energies of the target orbitals generated in SCF model. The nonrelativistic modified BEB ionization cross section [55] for each molecular orbital as a function of the incident energy T (< 10 KeV) is given by

$$\sigma_i(t) = \frac{S}{t + (u + 1)/np} \left\{ \frac{1}{2} \left(1 - \frac{1}{t^2} \right) \ln t + \left[\left(1 - \frac{1}{t} \right) - \frac{\ln t}{t + 1} \right] \right\}, \quad (2)$$

where $t = T/B$, $u = U/B$, and $S = 4\pi a_0^2 N(R/B)^2$. Here R is the Rydberg energy, B is the vertical ionization energy or the Binding energy, U is the orbital kinetic energy, N is the occupation number, and np is the principal quantum number of an orbital. The total cross section is the sum of cross sections of individual molecular orbitals. The np contributes significantly when its greater than or equal to 3, otherwise its contribution is taken as 1. At $T < B$, $\sigma_i(t) = 0$ as the molecular orbitals can not be ionized.

The molecular orbital data used in calculation of modified BEB cross section PO₂ is given in Table VIII. The modified BEB cross sections are shown in Fig. 6 from threshold

TABLE V. Feshbach resonances in resonating states 1B_1 and 3B_1 .

Resonating state configuration	E_r (eV)	Γ_r (eV)	Parent state
$^1B_1 : (\dots)7a_1^23b_1^19a_1^1$	4.99	0.044	$1^2B_1(8a_1 \rightarrow 3b_1)$
$^3B_1 : (\dots)7a_1^23b_1^19a_1^1$	4.95	0.011	$1^2B_1(8a_1 \rightarrow 3b_1)$
$^1B_1 : (\dots)1a_2^18a_1^19a_1^16b_2^1$	5.42	0.017	$2^2A_2(1a_2 \rightarrow 9a_1)$
$^3B_1 : (\dots)1a_2^18a_1^19a_1^16b_2^1$	5.35	0.014	$2^2A_2(1a_2 \rightarrow 9a_1)$
$^1B_1 : (\dots)8a_1^15b_2^13b_1^16b_2^1$	5.59	0.011	$3^2A_2(5b_2 \rightarrow 3b_1)$
$^3B_1 : (\dots)8a_1^15b_2^13b_1^16b_2^1$	5.44	0.014	$3^2A_2(5b_2 \rightarrow 3b_1)$
$^1B_1 : (\dots)2b_1^16b_2^2$	6.59	0.013	$4^2A_2(2b_1 \rightarrow 6b_2)$
$^3B_1 : (\dots)2b_1^16b_2^2$	6.39	0.0515	$4^2A_2(2b_1 \rightarrow 6b_2)$
$^1B_1 : (\dots)5b_2^13b_1^19a_1^16b_2^1$	6.63	0.018	$5^2A_2(5b_2 \rightarrow 3b_1, 8a_1 \rightarrow 9a_1)$
$^3B_1 : (\dots)5b_2^13b_1^19a_1^16b_2^1$	6.59	0.029	$5^2A_2(5b_2 \rightarrow 3b_1, 8a_1 \rightarrow 9a_1)$
$^1B_1 : (\dots)1a_2^29a_1^13b_1^1$	5.84	0.022	$3^2A_1(8a_1 \rightarrow 9a_1)$
$^3B_1 : (\dots)1a_2^29a_1^13b_1^1$	5.58	0.023	$3^2A_1(8a_1 \rightarrow 9a_1)$
$^1B_1 : (\dots)7a_1^18a_1^13b_1^19a_1^1$	6.41	0.059	$4^2B_1(7a_1 \rightarrow 3b_1)$
$^3B_1 : (\dots)7a_1^18a_1^13b_1^19a_1^1$	5.97	0.441	$4^2B_1(7a_1 \rightarrow 3b_1)$

TABLE VII. Feshbach resonances in resonating states 1A_2 and 3A_2 .

Resonating state configuration	E_r (eV)	Γ_r (eV)	Parent state
$^1A_2 : (\dots)1a_2^18a_1^19a_1^13b_1^1$	5.05	0.019	$2^2A_2(1a_2 \rightarrow 9a_1)$
$^3A_2 : (\dots)1a_2^18a_1^19a_1^13b_1^1$	5.01	0.025	$2^2A_2(1a_2 \rightarrow 9a_1)$
$^1A_2 : (\dots)6b_2^13b_1^1$	5.19	0.014	$3^2B_2(8a_1 \rightarrow 6b_2)$
$^3A_2 : (\dots)6b_2^13b_1^1$	5.17	0.015	$3^2B_2(8a_1 \rightarrow 6b_2)$
$^1A_2 : (\dots)5b_2^18a_1^19a_1^13b_1^1$	5.81	0.016	$4^2B_2(5b_2 \rightarrow 9a_1)$
$^3A_2 : (\dots)5b_2^18a_1^19a_1^13b_1^1$	5.80	0.021	$4^2B_2(5b_2 \rightarrow 9a_1)$
$^1A_2 : (\dots)7a_1^18a_1^13b_1^16b_2^1$	6.73	0.027	$4^2B_1(7a_1 \rightarrow 3b_1)$
$^3A_2 : (\dots)7a_1^18a_1^13b_1^16b_2^1$	6.71	0.081	$4^2B_1(7a_1 \rightarrow 3b_1)$
$^1A_2 : (\dots)2b_1^16b_2^19a_1^1$	6.51	0.0147	$4^2A_2(2b_1 \rightarrow 6b_2)$
$^3A_2 : (\dots)2b_1^16b_2^19a_1^1$	6.50	0.029	$4^2A_2(2b_1 \rightarrow 6b_2)$
$^1A_2 : (\dots)5b_2^18a_1^13b_1^19a_1^1$	5.64	0.0216	$3^2A_2(5b_2 \rightarrow 3b_1)$
$^3A_2 : (\dots)5b_2^18a_1^13b_1^19a_1^1$	5.62	0.015	$3^2A_2(5b_2 \rightarrow 3b_1)$
$^1A_2 : (\dots)5b_2^13b_1^19a_1^2$	6.68	0.027	$5^2A_2(5b_2 \rightarrow 3b_1, 8a_1 \rightarrow 9a_1)$
$^3A_2 : (\dots)5b_2^13b_1^19a_1^2$	6.66	0.005	$5^2A_2(5b_2 \rightarrow 3b_1, 8a_1 \rightarrow 9a_1)$

TABLE VIII. PO_2 molecular orbital binding and average kinetic energies (in eV).

Molecular orbital	$ B $	U	N
$1a_1$	2179.97	2889.966	2
$2a_1$	560.74	794.696	2
$3a_1$	207.99	431.536	2
$4a_1$	150.63	402.091	2
$5a_1$	38.39	75.268	2
$6a_1$	20.51	73.307	2
$7a_1$	16.85	53.696	2
$8a_1$	6.448	56.656	1
$1b_1$	150.67	401.657	2
$2b_1$	16.52	51.829	2
$1b_2$	560.74	794.689	2
$2b_2$	150.65	401.903	2
$3b_2$	36.94	80.349	2
$4b_2$	17.24	70.905	2
$5b_2$	14.41	60.826	2
$1a_2$	14.20	58.318	2

(10.6 eV) to 5000 eV. At high values of T , the cross sections show $\ln E/E$ behavior. The ionization cross sections show maximum at 67.05 eV energy.

C. Differential cross section

The differential cross section (DCS) for polar molecules is given as [56]

$$\frac{d\sigma}{d\Omega} = \frac{d\sigma^b}{d\Omega} + \sum_L (A_L - A_L^b) P_L(\cos \theta), \quad (3)$$

where the superscript b denotes that the Born approximation and P_L is a Legendre function. This expansion includes the contributions from higher partial waves and is dominated by the electron-dipole interaction. The quantity $d\sigma^b/d\Omega$ between

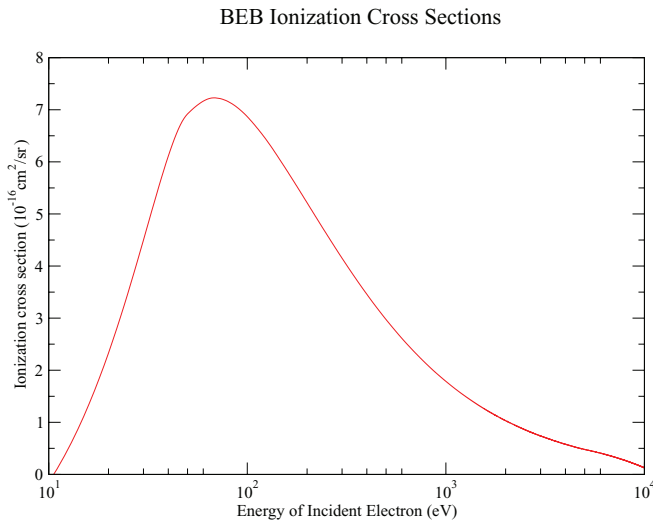


FIG. 6. (Color online) Electron impact BEB ionization cross sections.

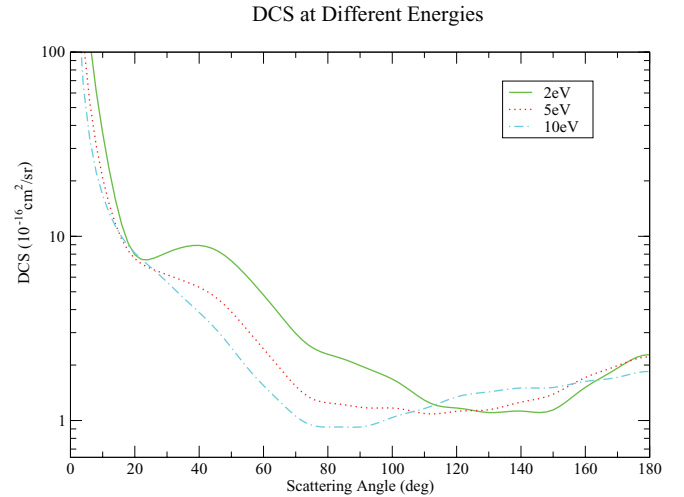


FIG. 7. (Color online) (a) Rotationally resolved state-to-state ($J \rightarrow J'$) cross sections at 5 eV in one-state model: thin dotted curve, $0 \rightarrow 0$; thin dashed curve, $0 \rightarrow 1$; big dashed curve, $0 \rightarrow 2$; dash-dotted curve, $0 \rightarrow 3$; double dash-dotted curve, $0 \rightarrow 4$; double dot-dashed curve, $0 \rightarrow 5$; thick curve, summed (over J') results.

initial $|J\tau\rangle$ and final rotor states $|J'\tau'\rangle$ is given by

$$\frac{d\sigma^b}{d\Omega} = \sum_{J'\tau'} \frac{d\sigma^b}{d\Omega}(J\tau \rightarrow J'\tau'). \quad (4)$$

The DCS are calculated using the POLYDCS program of Sanna and Gianturco [58]. These calculations are done at CI one-state level as the code is not applicable for closed channels, which appear for multistate coupling approximations. The rotational constants $A = 3.442\,359\,7439\, \text{cm}^{-1}$, $B = 0.286\,260\,0297\, \text{cm}^{-1}$, and $C = 0.264\,282\,7809\, \text{cm}^{-1}$ obtained are in excellent agreement with reported values [25,57]. The rotationally resolved differential cross sections at incident energy of 5 eV are shown in Fig. 7 while Table IX shows the rotational energy levels. The differential cross sections at small scattering angles are dominated by the dipole interaction and long-range polarization. The elastic component $0 \rightarrow 0$ and the dipole component $0 \rightarrow 1$ dominate over other values of J' . The rotationally summed DCS for all processes from $J = 0 \rightarrow J'(0-5)$ at 2, 5 and 10 eV are shown in Fig. 8. The sharp rise in DCS at very small scattering angles is due to the dipolar nature of the target. The singularity in DCS occurs as the scattering angle $\theta \rightarrow 0$. The DCS are also used to calculate the momentum-transfer cross section (MTCS), which are DCS weighted by a factor of $1 - \cos \theta$. The R -matrix calculations directly yield elastic cross sections, which match closely with that obtained by integrating DCS.

The MTCS obtained decrease with increasing energy as shown in Fig. 9. The MTCS are also useful in solving the Boltzmann equation for the electron distribution function. The Table X shows the variation of total elastic cross sections and MTCS at different energies in many-states model.

D. Effective collision frequency of electrons

Assuming the electrons to follow the Maxwell-Boltzmann distribution law, the effective electron- PO_2 collision frequen-

TABLE IX. Rotational energy levels.

J'	τ'	Energy (meV)
0	0	0.0
1	-1	0.068 259
1	0	0.459 570
1	1	0.462 29
2	-2	0.204 764
2	-1	0.593 36
2	0	0.601 538
2	1	1.775 5
2	2	1.775 48
3	-3	0.409 48
3	-2	0.794 045
3	-1	0.810 39
3	0	1.980 25
3	1	1.980 3
3	2	3.943 62
3	3	3.943 6
4	-4	0.682 380
4	-3	1.061 6
4	-2	1.088 85
4	-1	2.253 3
4	0	2.253 49
4	1	4.216 7
4	2	4.216 68
4	3	6.965 4
4	4	6.965 37
5	-5	1.023 4
5	-4	1.396 03
5	-3	1.436 9
5	-2	2.594 54
5	-1	2.595 0
5	0	4.558 03
5	1	4.558 0
5	2	7.306 70
5	3	7.306 7
5	4	10.840 7
5	5	10.841

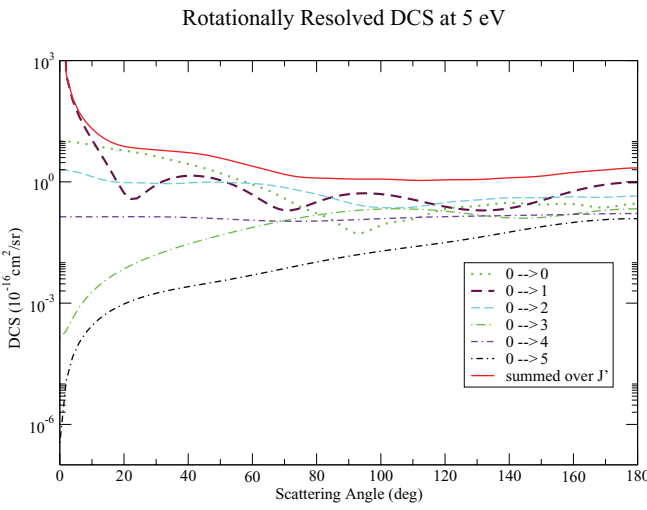
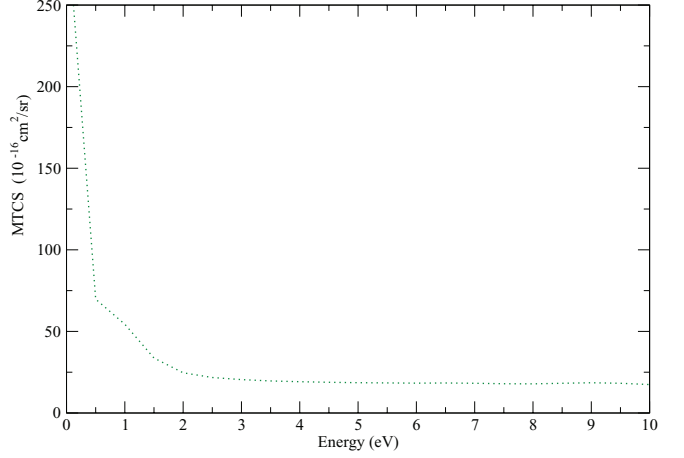
FIG. 8. (Color online) Summed rotationally resolved DCS at 5 eV. The plot shows DCS (10⁻¹⁶ cm²/sr) on a logarithmic y-axis (from 10⁻⁶ to 10³) versus Scattering Angle (deg) on the x-axis (from 0 to 180). Six curves are shown: 0 → 0 (dotted), 0 → 1 (dash-dotted), 0 → 2 (dashed), 0 → 3 (dash-dot-dotted), 0 → 4 (dash-dot), and 0 → 5 (solid). The solid curve is labeled "summed over J".

FIG. 9. (Color online) Momentum transfer cross sections.

cies such as $\langle v \rangle$ and \bar{v}^{-1} [59] can be expressed as

$$\langle v \rangle = \frac{8}{3\pi^{1/2} N} \left(\frac{m_e}{2kT_e} \right)^{5/2} \int_0^\infty v^5 Q^m(v) e^{-\frac{m_e v^2}{2kT_e}} dv \quad (5)$$

and

$$\bar{v}^{-1} = \frac{8}{3\pi^{1/2} N} \left(\frac{m_e}{2kT_e} \right)^{5/2} \int_0^\infty \frac{v^3}{Q^m(v)} e^{-\frac{m_e v^2}{2kT_e}} dv. \quad (6)$$

Here, N is the number density of molecules, m_e is the electron mass, k is the Boltzmann factor, T_e is electron temperature, v is the velocity of the electron, and $Q^m(v)$ is the velocity-dependent MTCS. The collision frequency is related to transport properties such as mean-free path, mobilities, and diffusion coefficients. The variation of $\langle v \rangle$ and \bar{v}^{-1} with temperature is shown in Fig. 10. Beyond 1000 K, they are almost same.

IV. CONCLUSION

A detailed analysis of electron impact on PO₂ radical is carried out using the *R*-matrix method. The various cross

TABLE X. Many-state elastic cross sections and MTCS at different energies.

Energy (eV)	MCI (a_0^2)	MTCS (10 ⁻¹⁶ cm ² /sr)
0.5	519.302 08	69.737 743
1.0	307.481 44	54.378 268
1.5	241.040	33.678 172
2.0	214.426 93	24.657 316
2.5	183.4928	21.752 655
3	164.720 54	20.447 255
3.5	151.579 75	19.655 277
4	142.7089	19.175 885
4.5	134.860 98	18.818 977
5	131.772 94	18.561 737
6	114.238 52	18.297 975
7	111.2003	18.227 696
10	102.761 43	17.427 244

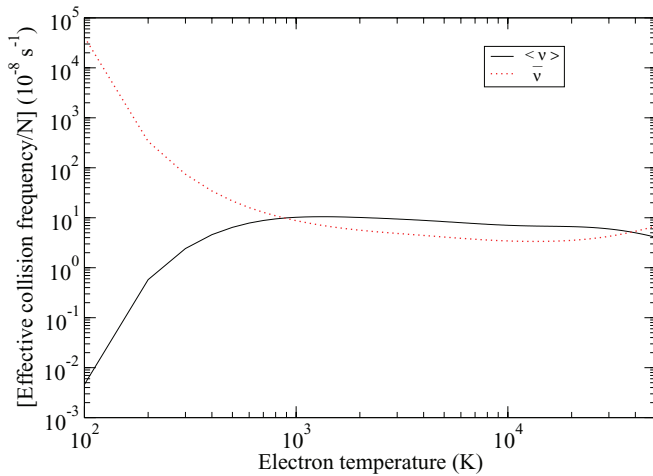


FIG. 10. (Color online) Effective collision frequency in ground state, solid curve, $\langle v \rangle$; dotted curve \bar{v} .

sections are reported. The values of ionization potential, electron affinity, vertical transition energy, dipole, and quadrupole moments of the target molecule have been satisfactorily obtained. The variations in the values of these quantities are due to the amount of correlation and polarization effects and the basis function used. The ROHF formalism yields good values of ionization potential from molecular orbital energies for the PO_2 radical. The data generated for MTCS can be used to calculate collision frequencies, which are useful for the evaluation of transport coefficients. The resonances discussed are real; while some of them are very narrow. Their parentage is carefully assigned by energetic and symmetry considerations. These resonances can not be termed as pseudoresonances as we have included all states below the highest electron energy studied. The correlation effects included in our calculations yield an accurate description of the resonance structure, exhibiting various types of resonances. They may be of immense use for dissociative electron attachment study.

- [1] B. Boudaiffa, P. Cloutier, D. Hunting, M. A. Huels, and L. Sanche, *Science* **287**, 1658 (2000).
- [2] S. Adhikari, *Variational Principles and the Numerical Solutions of Scattering Process* (Wiley, New York, 1998).
- [3] W. M. Huo and F. A. Gianturco, *Computational Methods for Electron-Molecule Collisions* (Plenum, New York, 1995).
- [4] O. P. Korobeinichev, S. B. Llyng, T. A. Bolshova, V. M. Shvartsberg, and A. A. Chernov, *Combust. Flame* **121**, 593 (2000).
- [5] A. Twarowksi, *Combust. Flame* **102**, 41 (1995).
- [6] E. J. P. Zegers and E. M. Fisher, *Combust. Flame* **115**, 230 (1998).
- [7] O. P. Korobeinichev, S. B. Llyng, V. M. Shvartsberg, and A. A. Chernov, *Combust. Flame* **118**, 718 (1999).
- [8] M. A. MacDonald, T. M. Jayaweera, E. M. Fisher, and F. C. Gouldin, *Combust. Flame* **116**, 166 (1999).
- [9] N. L. Howarth, G. B. Bacskay, and J. C. Mackie, *J. Phys. Chem. A* **106**, 1533 (2002).
- [10] M. E. Fraser and D. H. Stedman, *J. Chem. Soc., Faraday Trans. 1* **79**, 527 (1983).
- [11] M. E. Fraser, D. H. Stedman, and T. M. Dunn, *J. Chem. Soc., Faraday Trans. 1* **80**, 285 (1984).
- [12] D. Harris, M. Chou, and T. Cool, *J. Chem. Phys.* **82**, 3502 (1985).
- [13] R. P. Kampf and J. M. Parson, *J. Chem. Phys.* **108**, 7595 (1998).
- [14] C. J. Cramer and G. R. Famini, *Chem. Phys. Lett.* **169**, 405 (1990).
- [15] J. S. Fransisco, *J. Chem. Phys.* **117**, 3190 (2002).
- [16] Y. Kabadj and J. Lievin, *Phys. Scr.* **40**, 259 (1989).
- [17] L. L. Lohr, *J. Phys. Chem.* **88**, 5569 (1984).
- [18] L. L. Lohr and R. C. Boehm, *J. Phys. Chem.* **91**, 3203 (1987).
- [19] S. A. Jarrett-Sprague, I. H. Hillier, and I. R. Gould, *Chem. Phys.* **140**, 27 (1990).
- [20] Z. Xianyi, W. Jun, W. Fei, and C. Zhifeng, *J. Mol. Struct., Theochem* **851**, 40 (2008).
- [21] C. Xu, E. de Beer, and D. M. Neumark, *J. Chem. Phys.* **104**, 2749 (1996).
- [22] Y. Pak and R. C. Wood, *J. Chem. Phys.* **104**, 5547 (1996).
- [23] Z. L. Cai, G. Hirsch, and R. J. Buenker, *Chem. Phys. Lett.* **255**, 350 (1996).
- [24] M. A. Lawson, K. J. Hoffman, and P. B. Davies, *J. Mol. Spectro.* **269**, 61 (2011).
- [25] K. Kawaguchi, S. Saito, E. Hirota, and N. Ohashi, *J. Chem. Phys.* **82**, 4893 (1985).
- [26] H. B. Qian, P. B. Davies, and P. A. Hamilton, *J. Chem. Soc., Faraday Trans.* **91**, 2991 (1995).
- [27] J. Lei, T. Teslja, B. Nizamov, and P. J. Dagdigian, *J. Phys. Chem. A* **105**, 7828 (2001).
- [28] P. A. Hamilton, *J. Chem. Phys.* **86**, 33 (1987).
- [29] L. Andrews, M. McCluskey, Z. Mielke, and R. Withnall, *J. Mol. Struct.* **222**, 95 (1990).
- [30] R. Withnall, M. McCluskey, and L. Andrews, *J. Phys. Chem.* **93**, 126 (1989).
- [31] R. D. Verma and C. F. McCarthy, *Can. J. Phys.* **61**, 1149 (1983).
- [32] L. B. Knight, G. C. Jones, G. M. King, R. M. Babb, and A. J. McKinley, *J. Chem. Phys.* **103**, 497 (1995).
- [33] M. McCluskey and L. Andrews, *J. Phys. Chem.* **95**, 2988 (1991).
- [34] Z. Mielke, M. McCluskey, and L. Andrews, *Chem. Phys. Lett.* **165**, 46 (1990).
- [35] L. A. Morgan, C. J. Gillan, J. Tennyson, and X. Chen, *J. Phys. B: At. Mol. Opt. Phys.* **30**, 4087 (1997).
- [36] L. A. Morgan, J. Tennyson, and C. J. Gillan, *Comput. Phys. Commun.* **114**, 120 (1998).
- [37] P. G. Burke, *R-Matrix Theory of Atomic Collisions: Application to Atomic, Molecular and Optical Processes* (Springer-Verlag, Berlin, 2011).
- [38] B. M. Nestmann, K. Pfingst, and S. D. Peyerimhoff, *J. Phys. B: At. Mol. Opt. Phys.* **27**, 2297 (1994).
- [39] T. H. Dunning and P. J. Hay, in *Methods of Electronic Structure Theory*, Vol. 2, edited by H. F. Schaefer (Plenum, New York, 1977).
- [40] R. O. Esquivel, J. C. Angulo, J. Antolin, J. S. Dehesa, S. Lopez-Rosa, and N. Flores-Gallegos, *Phys. Chem. Chem. Phys.* **12**, 7108 (2010).

- [41] B. N. Plakhutin, E. V. Gorelik, and B. N. Breslavskaya, *J. Chem. Phys.* **125**, 204110 (2006).
- [42] O. P. Korobeinnichev, V. M. Shvartsberg, and A. A. Chernov, *Combust. Flame* **118**, 727 (1999).
- [43] S. G. Lias, J. E. Bartmess, J. F. Liebman, J. L. Holmes, R. D. Levin, and W. G. Mallard, *J. Phys. Chem. Ref. Data* **17**, Suppl. 1 (1988).
- [44] O. P. Korobeinnichev, V. M. Shvartsberg, and A. G. Shmakov, *Russian J. Phys. Chem. B* **2**, No. 6, 856 (2008).
- [45] A. I. Fernandez, A. J. Midey, T. M. Miller, and A. A. Viggiano, *J. Phys. Chem. A* **108**, 9120 (2004).
- [46] E. P. F. Lee, D. K. W. Mok, J. M. Dyke, and F. Chau, *J. Phys. Chem. A* **106**, 10130 (2002).
- [47] A. Faure, J. D. Gorfinkel, L. A. Morgan, and J. Tennyson, *Comput. Phys. Commun.* **144**, 224 (2002).
- [48] S. Kaur, K. L. Baluja, and J. Tennyson, *Phys. Rev. A* **77**, 032718 (2008).
- [49] S. Kaur and K. L. Baluja, *Phys. Rev. A* **80**, 042701 (2009).
- [50] T. D. Mark and G. H. Dunn, *Electron Impact Ionization* (Springer, Wien, 1985).
- [51] R. K. Janev, *Atomic and Molecular Processes in Fusion Edge Plasma* (Plenum, New York, 1995).
- [52] V. Tarnovsky and K. Becker, *Plasma Sources Sci. Technol.* **4**, 307 (1995).
- [53] Y. K. Kim and M. E. Rudd, *Phys. Rev. A* **50**, 3954 (1994).
- [54] W. Hwang, Y. K. Kim, and M. E. Rudd, *J. Chem. Phys.* **104**, 2956 (1996).
- [55] Y. K. Kim, W. Hwang, N. M. Weinberger, M. A. Ali, and M. E. Rudd, *J. Chem. Phys.* **106**, 1026 (1997).
- [56] S. Kaur, Anand Bharadvaja, and K. L. Baluja, *Phys. Rev. A* **83**, 062707 (2011).
- [57] H. B. Qian, P. B. Davies, I. K. Ahmed, and P. A. Hamilton, *Chem. Phys. Lett.* **235**, 255 (1995).
- [58] N. Sanna and F. A. Gianturco, *Comput. Phys. Commun.* **114**, 142 (1998).
- [59] P. Baille, J. S. Chang, A. Claude, R. M. Hobson, G. L. Ogram, and A. W. Yau, *J. Phys. B: At. Mol. Phys.* **14**, 1485 (1981).